Behaviour of two reinforced test embankments on soft clay

H. O. Magnani[1], M. S. S. Almeida[2] and M. Ehrlich[3]

[1]*Department of Civil Engineering, Federal University of Santa Catarina, Rua João Pio Duarte da Silva, n° 205, Carrego Grande, Florianópolis, Santa Catarina, CEP: 88040-970, Brazil, Telephone: +55 21 3224 5986; Telefax: +55 21 2562 7200; E-mail: henriquemagnani@uol.com.br*
[2]*Graduate School of Engineering, COPPE, Federal University of Rio de Janeiro, Caixa Postal 68506, CEP 21945, Rio de Janeiro, RJ, Brazil, Telephone: +55 21 2562 7772; Telefax: +55 21 2562 7200; E-mail: almeida@coc.ufrj.br*
[3]*Graduate School of Engineering, COPPE, Federal University of Rio de Janeiro, Caixa Postal 68506, CEP 21945, Rio de Janeiro, RJ, Brazil, Telephone: +55 21 2562 7193; Telefax +55 21 2562 7200; E-mail; me@coc.ufrj.br*

Received 23 September 2008, revised 13 January 2009, accepted 18 January 2009

ABSTRACT: The paper presents the behaviour of two reinforced test embankments built on a normally consolidated soft clay deposit underlying a top sand layer. The embankments were constructed close to undrained conditions in about 60 days. The embankments were well instrumented, including measurements of tension forces in the reinforcement. The mobilised tension forces in the reinforcements were shown to increase with embankment height and larger values of tension forces were measured in the embankment built on a shallower clay layer. The critical failure surfaces obtained in limit equilibrium stability analyses were close to the observed field failure surfaces. These analyses used measured reinforcement forces and resulted in Bjerrum correction factors around $\mu = 0.60$ for the two embankments. These analyses considered the measured reinforcement forces and three-dimensional effects. Consistent correlations were obtained between embankment loadings, factors of safety, measured reinforcement forces and inclinometer readings.

KEYWORDS: Geosynthetics, Embankment, Reinforcement, Soft clay, Stability

REFERENCE: Magnani, H. O., Almeida, M. S. S. and Ehrlich, M. (2009). Behaviour of two reinforced test embankments on soft clay. *Geosynthetics International*, **16**, No. 3, 127–138.
[doi: 10.1680/gein.2009.16.3.127]

1. INTRODUCTION

Embankments on soft clays very often use basal reinforcement to increase the factor of safety against failure (Rowe and Li 2005). The three typical modes of failure of reinforced embankments on soft soils are: internal or lateral spreading failure; bearing or foundation failure; and global or overall failure, which includes both embankment and foundation (Bonaparte and Christopher 1987; Jewell 1992). The mode of failure of main interest herein is foundation failure as there was no basal reinforcement failure in the present case studies.

A number of methods can be used for stability analysis of reinforced embankments with the purpose of defining the tensile force of the reinforcement. Some of these methods use circular or non-circular surfaces (e.g. Milligan and Busbridge 1983; Leshchinsky 1987; Low *et al*. 1990; Kaniraj 1994), analytical solutions or plasticity theory (Davis and Booker 1973; John 1987; Houlsby and Jewell 1988; Jewell 1996), or limit equilibrium methods (Long *et al*. 1996; Bergado *et al*. 2002; Shukla and Kumar 2008). These methods do not take into account the relative displacements and strains in the clay and reinforcement, which are responsible for the actual mobilised force in the reinforcement (Rowe and Soderman 1985). In order to obtain the necessary factor of safety, the computed reinforcement forces may be quite high using these methods. However, these forces may not necessarily be mobilised in situ due to insufficient strain in the reinforcement. Consequently, the actual factor of safety in situ may be quite low and differ from the calculated values, thus leading to excessive displacements or failure of the embankment. In order to overcome these difficulties, some methods have been proposed to estimate the reinforcement forces by considering the deformability parameters of both the reinforcement and the soft clay (e.g. Rowe and Soderman 1985). Alternatively, numerical methods, most commonly using finite elements

(e.g. Li and Rowe 2001; Tanchaisawat *et al*. 2008), may be used for the same purpose.

The mechanisms involved in the mobilised forces in reinforced embankments on soft clays are discussed in this paper. The analysis is based on two reinforced test embankments taken to failure on a soft normally consolidated clay deposit. Emphasis is given to the results of the measured reinforcement forces and the relationship of these forces with the inclinometer measurements and computed factors of safety.

2. TEST EMBANKMENT

2.1. Historical background

In the mid-1990s, a hydraulic embankment was built as the first construction phase of a motorway near the shore in the city of Florianópolis located in southern Brazil over 4 to 22 m of soft clay deposit. This hydraulic fill, with a thickness varying from 0 to 5.5 m, was used to raise the ground level above sea level so that construction could continue using standard fill construction methods. Although it was generally successful, some failures occurred, which suggested the need for a more detailed study to investigate the continuity of the embankment construction. Therefore, in late 2002, three test embankments were constructed; two of which were reinforced and the third one was not (Magnani 2006). The unreinforced embankment had a much shallower clay layer and also a sand lens in the middle, and thus it could not serve as a reference for comparison with the two reinforced embankments. Magnani (2006) has described the overall behaviour of the three test embankments; the present paper reports on further investigation of the behaviour of the two reinforced embankments.

2.2. Soils, reinforcement and drains

Table 1 presents a summary of the main geotechnical characteristics of Florianópolis soft clay. The geotechnical parameters of this very soft clay are typical of the Brazilian coastal marine deposits. The soft clay under the test embankment demonstrates the behaviour of a normally consolidated clay deposit owing to the construction of the hydraulic fill working platform 6 years before the construction of the test embankments.

The test embankments were constructed with different features in order to yield relevant data for the motorway construction. Test embankment 1 (TE1) included both vertical drains and reinforcement, as is generally adopted in motorways, whereas test embankment 2 (TE2) was constructed with reinforcement only. Test embankment 3 (TE3), which had neither drains nor reinforcement, was also built, but this is not addressed in the present paper (Magnani 2006). Table 2 presents the main features of the two reinforced test embankments. Note that although the embankments were located quite close to one another, the thicknesses of the underlying soft clay layers were quite different.

Undrained strength profiles at the centre of each embankment are presented in Figure 1. These continuous profiles were computed with the equation $S_u = (q_T - \sigma_v)/N_{kt}$ (Lunne *et al.* 1997), where S_u is the (uncorrected) vane strength, q_T is the corrected point resistance, σ_v is the total vertical stress, and N_{kt} is the empirical cone factor. The value $N_{kt} = 12.0$ was adopted, based on correlations (Magnani 2006) between a number of vane and piezocone tests that were performed at the test site.

Table 1. Geotechnical parameters of Florianópolis soft clay

Parameter	Value
Water content w (%)	100–170
Liquidity index w_P (%)	105–165
Average plasticity index I_P (%)	80
Bulk unit weight γ_b (kN/m^3)	13.2–14.2
Void ratio e	2.9–4.5
Compression ratio $C_c/(1 + e_o)$	0.30–0.45
Coefficient of vertical consolidation c_v, normally consolidated (m^2/s)	$0.7–1.0 \times 10^{-8}$
Sensitivity (vane)	3–6

Table 2. Main features of the two reinforced embankments

	Embankment	
	TE1	TE2
Reinforcement	Polyester Stabilenka 200 kN/m × 45 kN/m; J = 1700 kN/m	
Vertical drains	Colbondrain CX 1000, 10 cm × 0.5 cm, triangular array, 1.30 m spacing	No drains
Clay thickness (m)	8.2	5.6
Working platform thickness (sand hydraulic fill) (m)	1.7	1.8

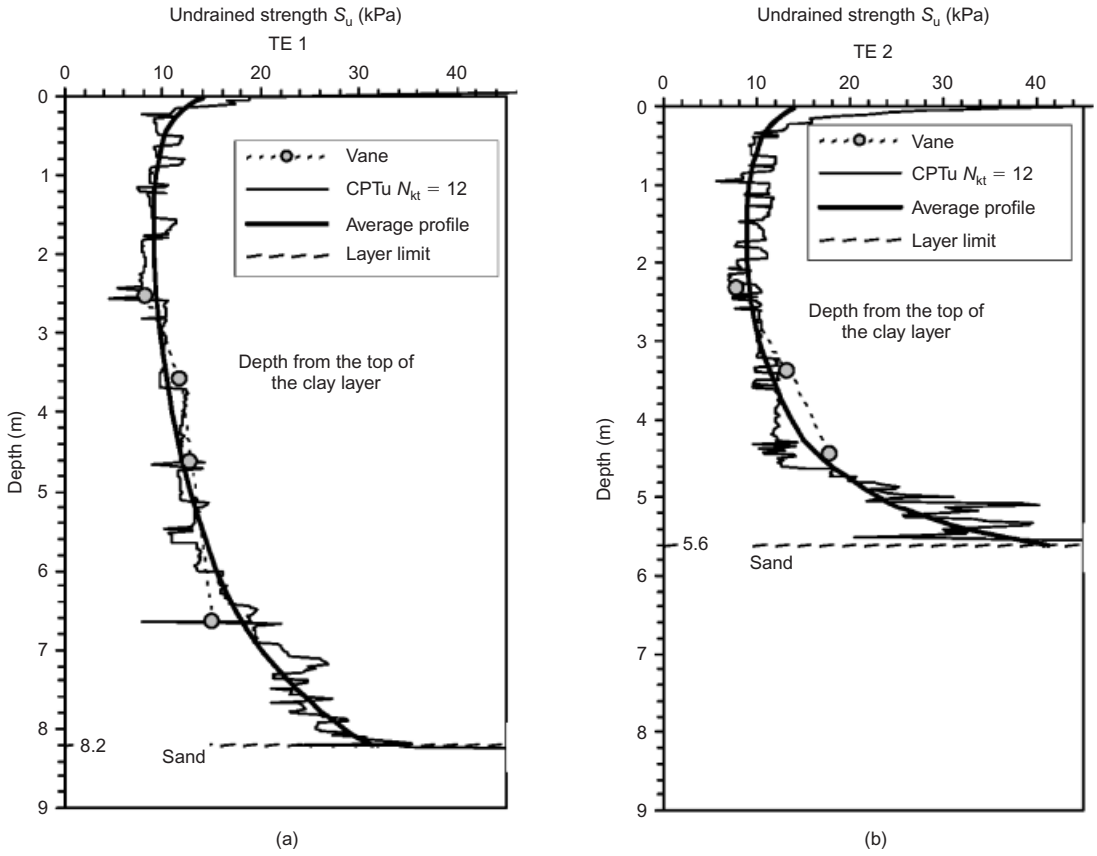

Figure 1. Undrained strength profiles at test embankments TE1 and TE2

2.3. Geometry and instrumentation

Figure 2 presents the cross-section of embankment TE1 (before and after failure) with slope 1 (V) : 1.5 (H). The two test embankments TE1 and TE2 were fully instrumented for vertical displacements (settlement plates, vertical extensometers, surface marks), horizontal displacements (Digitilt Datamate Slope Indicator), pore pressures (vibrating wire piezometers), and also tension forces at the reinforcement. For the present paper the relevant measurements were horizontal displacements and reinforcement

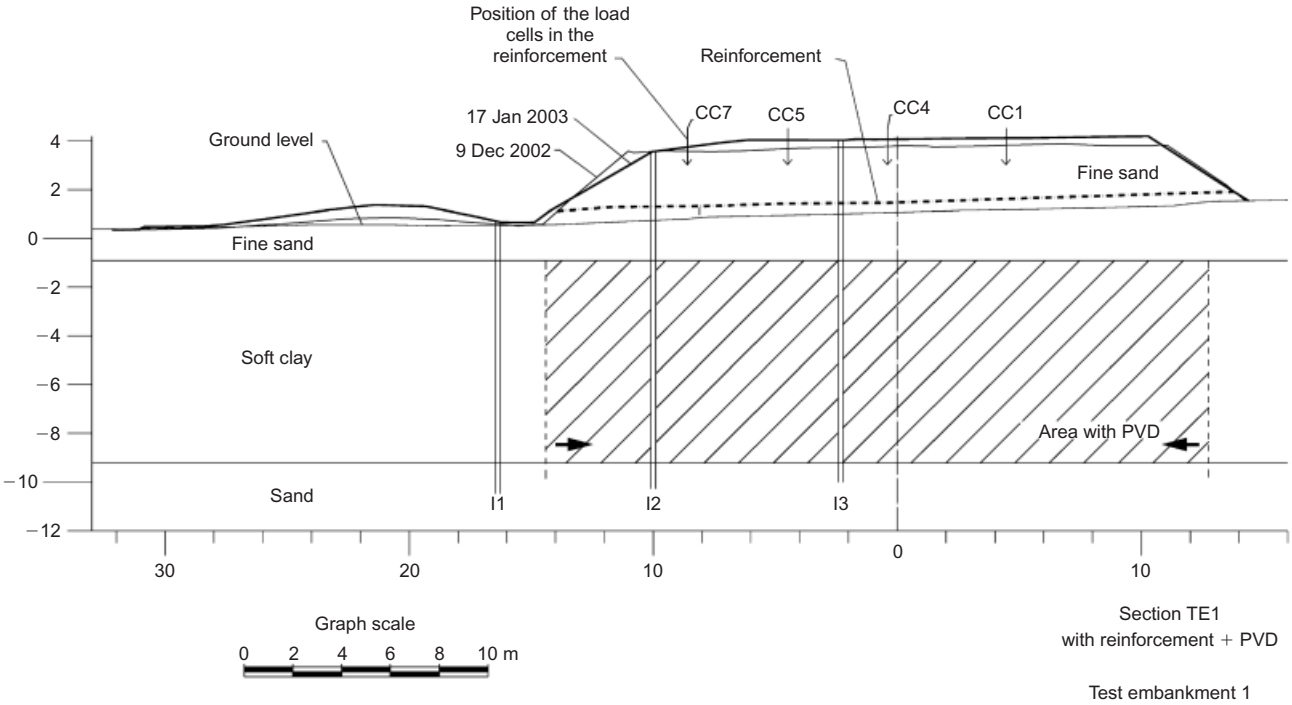

Figure 2. Embankment geometry and instrumentation analysed

forces and these are shown in Figure 2 for test embankment TE1.

Test embankment TE2 had essentially the same geometry, position of load cells, and position of inclinometers as TE1. As mentioned before, TE2 did not have vertical drains and the soft clay layer was less thick. The platform in plan view was 20 m in width (see Figure 2) and 30 m in length. In addition, lateral berms 12 m in length at each side and 1 m high were also provided. The overall geometry allowed plane strain conditions and induced failure in the central region. The direction of the failure was naturally induced by the gentle inclination of the embankment base. The test embankments were constructed in 60 days.

Reinforcement forces were measured at four points in the reinforcement (see Figure 2). The load cells used to monitor reinforcement forces (Magnani 2006) have been used in a number of studies carried out at COPPE in recent years (e.g. Saramago 2002; Saramago and Ehrlich 2005).

Overall analysis of the instrumentation of the two embankments has been presented by Magnani (2006). The two embankments presented behaviour that was typical of undrained conditions. Therefore, soil heave in front of the embankment was slightly smaller than settlements under the embankment. Generated pore pressures during embankment construction were close to the vertical applied load for embankment TE2 and slightly smaller for embankment TE1 with vertical drains.

It was estimated (Magnani 2006) that the contributions of the drains to the average gains in strength just before failure (about 60 days from beginning of construction) were 2.1 kPa for TE1 and 0.8 kPa for TE2. The estimated consolidation settlements before failure (eighth layer) were 0.28 m for embankment TE1 and 0.08 m for embankment TE2. The generated pore pressure under embankment TE1 was slightly less than under embankment TE2. Therefore, for the purpose of the analyses carried out in the present study, the influence of the vertical drains was relatively small.

3. EMBANKMENT BEHAVIOUR

3.1. Horizontal displacements

The inclinometer measurements in both embankments are shown in Figure 3. These measurements are related to the inclinometers located at the embankment toe which presented the largest measured values, as expected. The results presented in Figure 3 are horizontal displacements δ_h and vertical deviation θ_v. The vertical deviation is defined as the increment in horizontal displacement $\Delta\delta_h$ divided by the distance between the measured points Δz, that is $\theta_v = \Delta\delta_h/\Delta z$. Horizontal displacements were greater in embankment TE1 where a thicker clay layer occurs (Magnani 2006). It was noted that both curves (δ_h and θ_v) had maintained their shapes as the embankment height increased, which confirms observations by Tavenas *et al.* (1979). The depth of the maximum vertical deviation is the depth of maximum shear strains and the depth of the failure surface. These depths were constant during the raising of the embankment and were 5.0 m for embankment TE1 and 3.8 m for embankment TE2. Embankment TE3 (without reinforcement) had the smallest clay thickness and the shallowest failure surface (Magnani 2006).

Figure 4 presents the results of maximum vertical deviation θ_{max} plotted against time for all inclinometers of embankments TE1 and TE2. The instant of greatest change in the inclination in the slope curves θ_{max} plotted against time is related to the construction of the ninth layer (see vertical lines in Figure 4) for both embankments. This threshold point virtually coincides in all the inclinometers and indicates the onset of failure of the clay foundation. In both embankments the eighth layer of construction may be considered the last stable condition. Owing to high levels of horizontal deformation it was not possible to insert the inclinometer sensor inside the inclinometer tube located at the toe of embankment TE1 after the eighth layer of construction. Cracks appeared in both embankments at the ninth layer of construction but failure was more clearly seen in the tenth layer in both embankments.

As shown in Figure 4, embankment TE2 presented a systematically larger vertical deviation than embankment TE1. This was attributed to the smaller thickness of the clay layer underneath the surface of embankment TE2 compared with the corresponding one of embankment TE1, thus generating a larger maximum vertical deviation. Note the very similar shapes of the curves of maximum vertical deviations plotted against time (Figure 4) and maximum horizontal displacements plotted against time shown in Figure 5.

3.2. Deformations in the embankment foundations

The responses of the clay layers under the embankment loadings were compared for the two embankments. With this purpose the embankment loading $\Delta\sigma_v$ (considering submersion due to settlement) was plotted against the maximum deviation θ measured at the embankment toe, as shown in Figure 6.

The curves fitting the data are also shown in Figure 6 and these are similar to stress–strain curves seen in undrained triaxial tests carried out in normally consolidated clays.

A very small difference (about 3 kPa) was verified between the curves of the two embankments. Therefore, it may be concluded from Figure 6 that the two reinforced embankments had a quite similar shearing response, despite the differences between the vertical drains and the thicker clay foundation at embankment TE1.

The maximum shear strains occurred under the embankment slope. Values of distortions γ were obtained in this region and were related to factors of safety. The distortion γ of a soil element resulting from changes in stresses is defined as the change in the angles that were originally square (see Figure 7), as defined by the equation

$$\gamma = \theta_v + \theta_h \quad (1)$$

where θ_v is the vertical deviation, and θ_h is the horizontal deviation.

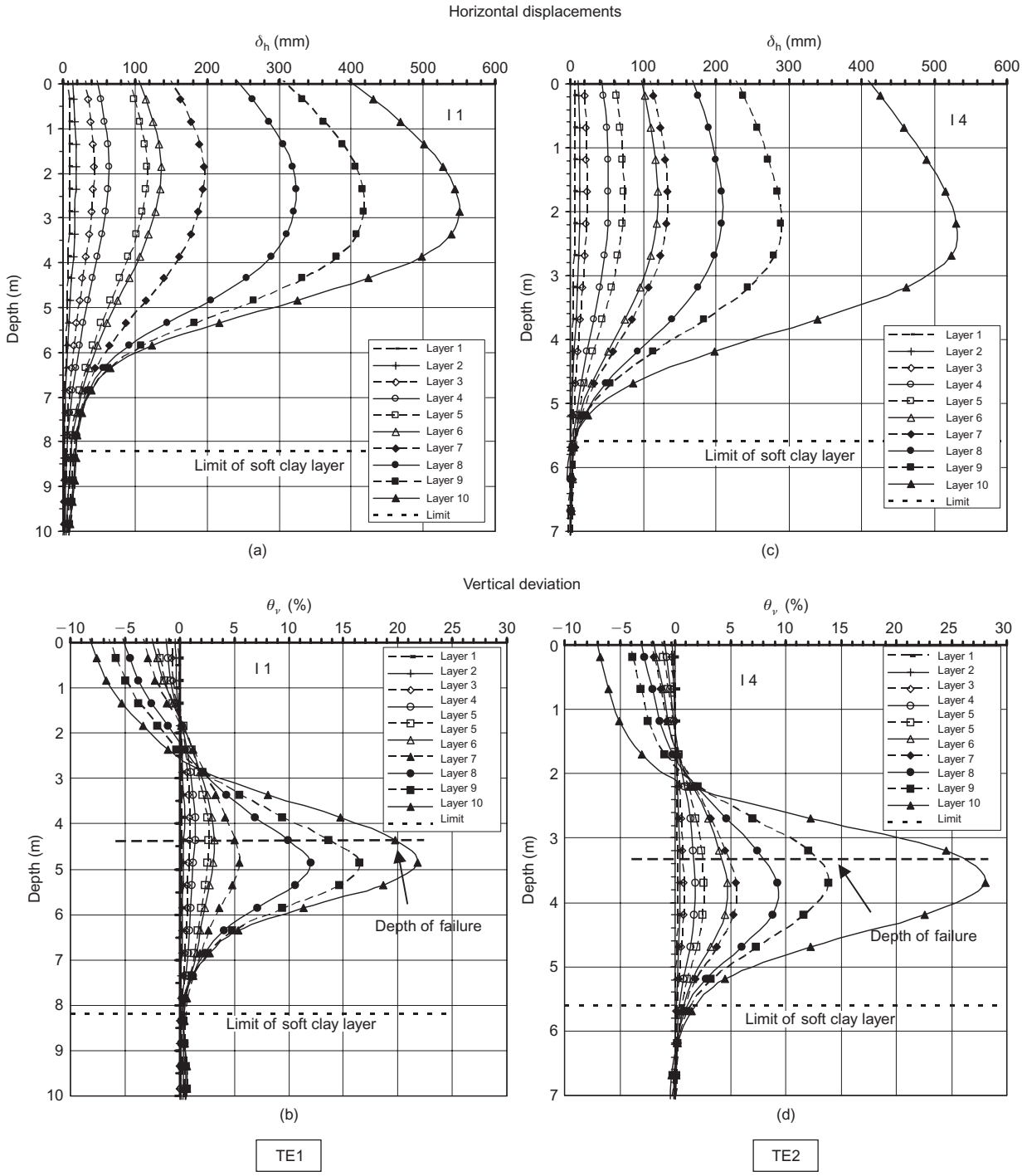

Figure 3. Toe inclinometer data for test embankments TE1 and TE2

The values of vertical deviation are shown in Figure 3 for the inclinometer at the toe of embankment TE1. Values of horizontal deviation computed by Magnani (2006) from settlement measurements in two vertical magnetic extensometers' located under the embankment near the toe are presented in Figure 8 for embankment TE1.

Profiles of distortion γ at the embankment toe for the two inclinometers are presented in Figure 9 for the two test embankments. It can be seen that the shapes of these curves are quite similar to those related to the vertical deviation shown in Figure 3.

3.3. Measured and estimated reinforcement forces

The values of forces measured at the four load cells installed in the reinforcement in embankments TE1 and TE2 are shown in Figure 10 for each fill layer. Note that the maximum reinforcement forces just after construction measured in embankment TE1 (Figure 10(a)) were close to the embankment toe, but in embankment TE2 (Figure 10(c)) these values were verified in the central region of the embankment. Further measurements in embankment TE1 (see Figure 10(c)) show that the pattern of measurements was

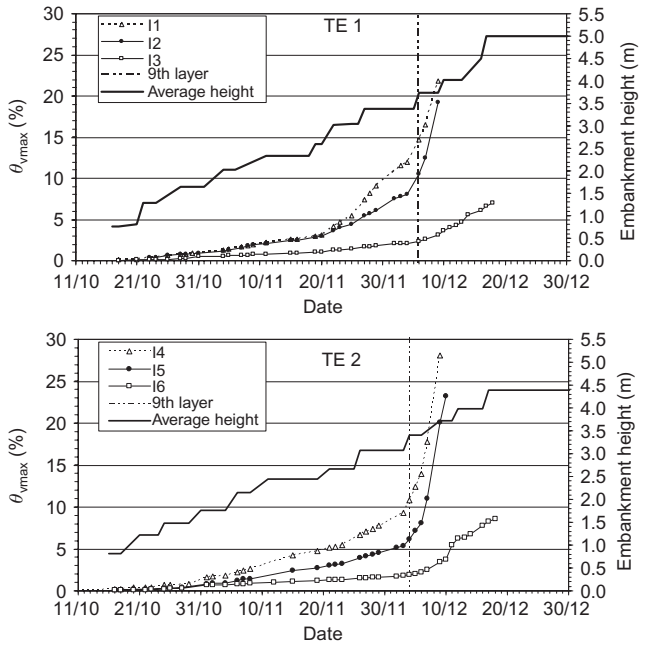

Figure 4. Maximum vertical deviation and embankment height plotted against time

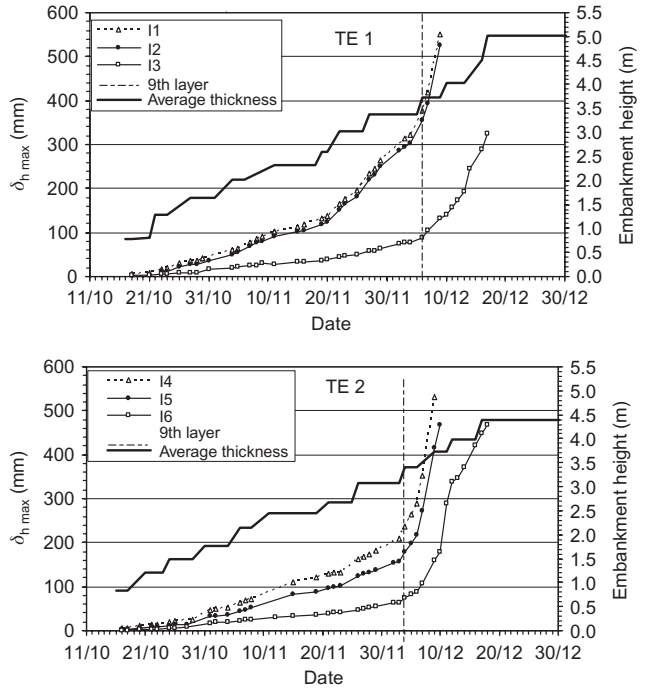

Figure 5. Maximum horizontal displacements and embankment height plotted against time

closer to the expected pattern and also to that of embankment TE2.

After the placement of the tenth fill layer, readings in some load cells (Figure 10(a), (b)) appear to indicate the failure of these load cell connections. The cells concerned were the first load cell in embankment TE1 and the second load cell in embankment TE2. Exhumation of the geotextiles indicated that these were in good condition and

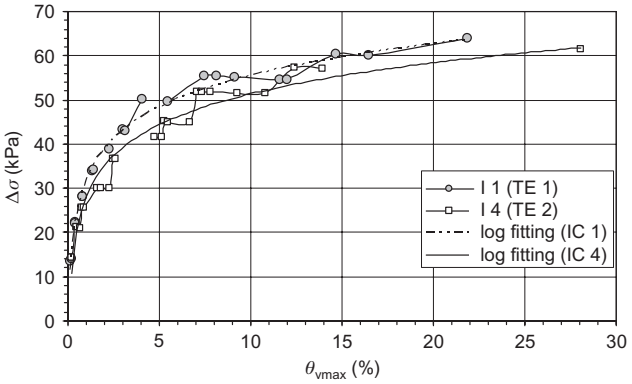

Figure 6. Embankment loading $\Delta\sigma_v$ plotted against vertical deviation for test embankments TE1 and TE2

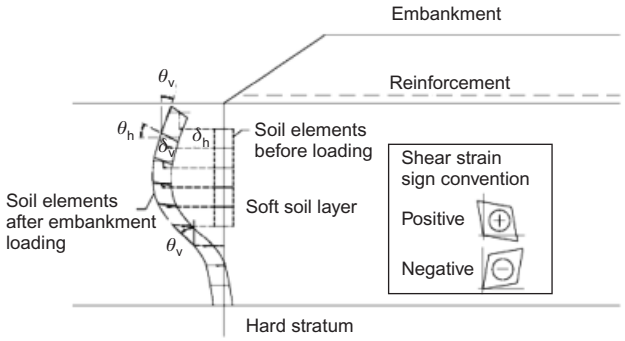

Figure 7. Displacements, rotations, and shear deformations of the elements under the embankment toe

also showed the failed connections of the two load cells described above.

Values of the reinforcement force T measured for different embankment loading conditions are shown in Table 3. The measured T values for the two embankments (TE1 and TE2) were quite close. The geotextile reinforcement strains ε_a computed from measured T values and reinforcement modulus $J = 1700$ kN/m are less than 0.5% in service conditions and in the range 0.6–1.1% at the onset of failure, reaching 2.4–3.0% when the embankment started to crack.

Values of reinforcement strains ε_a and measured reinforcement forces T in failure conditions were computed using Rowe and Soderman's method (Rowe and Soderman 1985). The parameters adopted in the calculations are presented in Table 4 together with the computed values of reinforcement strains and forces. The computed strain values ε_a were in the range 1.6–3.5%, which is of the same order of magnitude as the field-estimated values of 2.4–3.0%. Thus the estimated T values, also presented in Table 4, were of the same order of magnitude as the measured values. The T values predicted by the Rowe and Soderman method were higher for embankment TE1 than for TE2, but the measured values indicated the opposite. The computed value of T at failure for embankment TE1 was close to $T = 70$ kN/m, as measured in this embankment after failure.

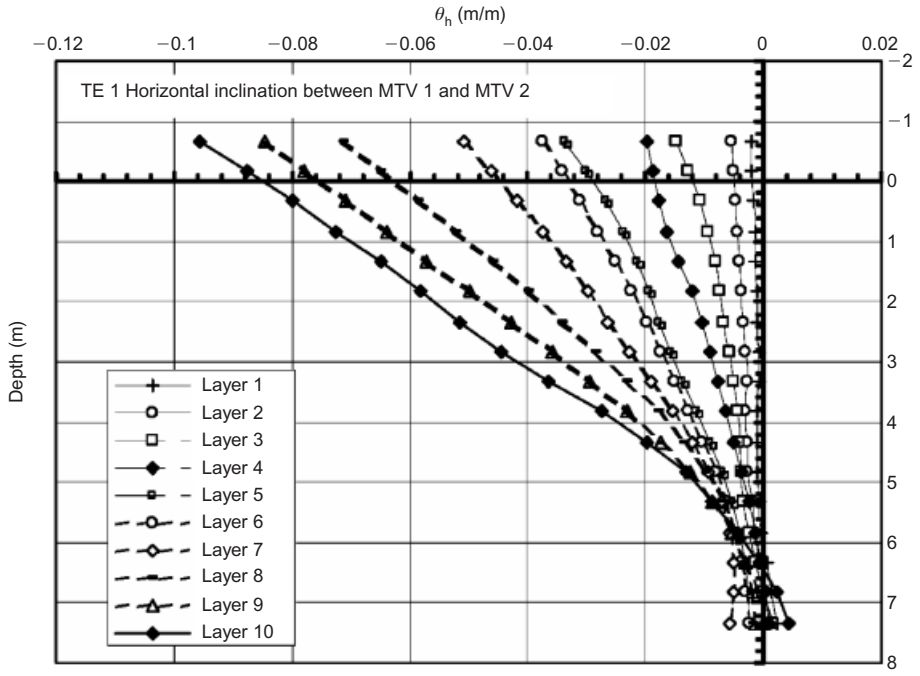

Figure 8. Horizontal deviation plotted against depth for test embankment TE1

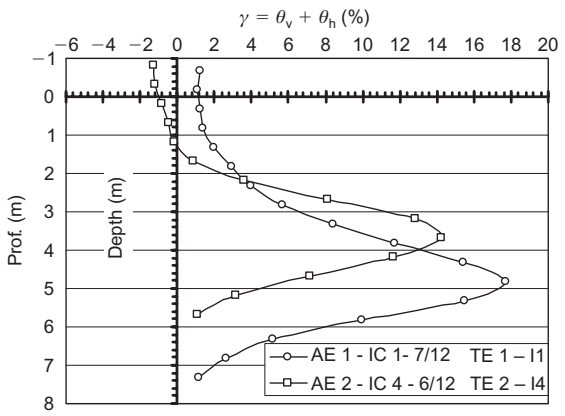

Figure 9. Distortions plotted against depth for embankments TE1 and TE2 for the ninth layer

3.4. Reinforcement forces versus inclinometer measurements and embankment loading

Figure 11 presents the values of the maximum reinforcement forces T measured with time and embankment height h for embankment TE1. Similar results were obtained for embankment TE2 (Magnani 2006). As expected, the measured values of T increased with h and, just after the ninth fill layer (vertical lines in Figure 11), which may be considered the moment at which failure occurred in both embankments, the values of T presented a greater rate of increase. A similar trend was also observed for the inclinometer measurements with time, as shown in Figures 4 and 5. However, the measured vertical deviation at the inclinometers appeared to be more sensitive to embankment loading than to reinforcement forces. These two sets of monitoring data were related, as shown in Figure 12 for the two embankments TE1 and TE2. Figure 12 shows a linear relationship between the maximum forces T_{max} measured at the central regions of the embankments, where the cracks appeared, and the maximum vertical deviation θ_{max} measured by the inclinometers located at the embankment toe. It is interesting to notice that the linear relationship was maintained not just in service conditions but at failure and even beyond failure, being valid for foundations with and without vertical drains. The linear relationship between these two variables confirms that the mobilised tension was directly related to measured deformations of the soft soil.

Graphs showing the measured tension in the reinforcement (T) plotted against the applied embankment load $\Delta\sigma_v$ for both embankments are presented in Figure 13. The values of T presented are those measured at the third load cell located in the centre of the embankment where the cracks appeared. It may be observed that greater values of T were mobilised in embankment TE2 than in embankment TE1. This may be attributed to the shorter distance between the failure surface and the base of the clay layer for embankment TE2 in comparison with TE1. Therefore, the gradient of the horizontal displacements is greater and so are the vertical deviation values, as explained earlier, and thus the T values are also greater.

4. STABILITY ANALYSES OF THE TEST EMBANKMENTS

4.1. Parameters and hypotheses

Stability analyses of the two test embankments were carried out based on the parameters shown in Table 5. The stability analyses carried out for each embankment layer used the values of the forces T measured in the load cells (see Figure 6).

The analyses took into account the deformed embankment geometry of each layer due to the overall embank-

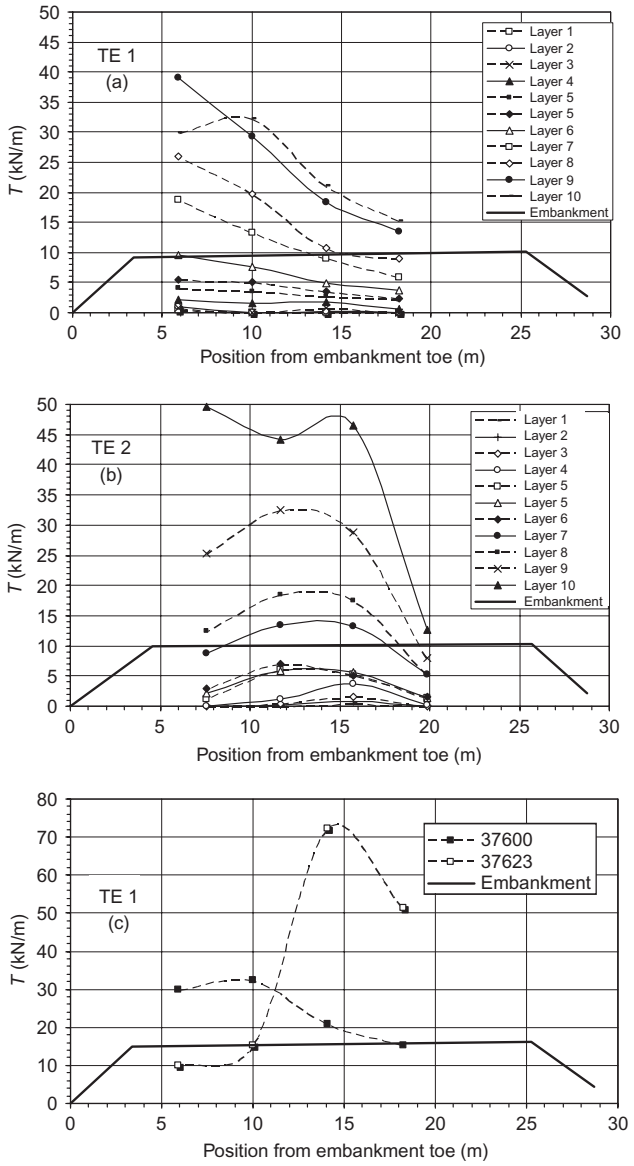

Figures 10. Measured reinforcement forces for each embankment layer

ment deformation. The reinforcement forces (T) used in the analyses were considered to act in the horizontal direction, the standard procedure in geotechnical practice. In the present cases, the maximum measured reinforcement rota-

Table 3. Values of the reinforcement force (*T*) measured for different embankment conditions

Embankment condition	Measured reinforcement forces, *T* (kN/m)	
	TE1	TE2
Service behaviour ($F_s \approx 1.4$)	4	7
Onset of failure	11–20	18
Embankment cracking	40	50
Maximum value after failure	–	70

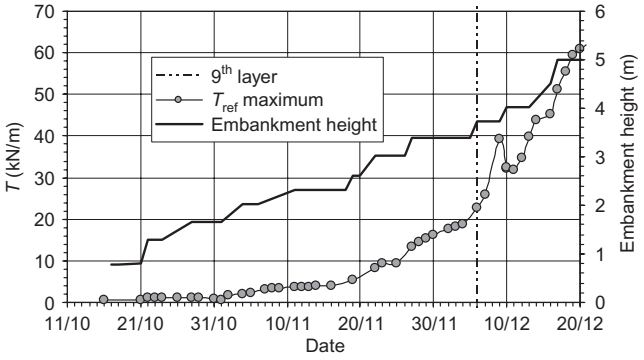

Figure 11. Reinforcement forces and embankment height plotted against time for test embankment TE1

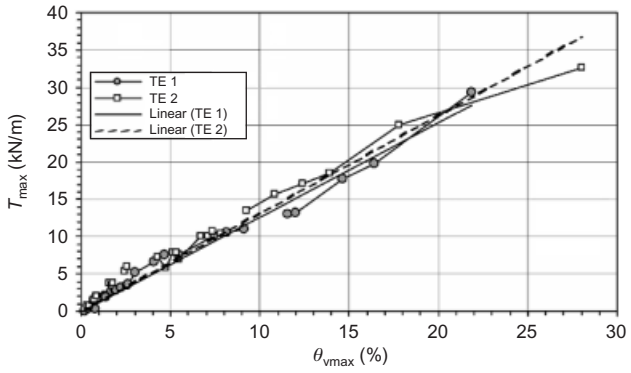

Figure 12. Maximum reinforcement forces plotted against maximum vertical deviation

Table 4. Strains and reinforcement forces estimated at failure using Rowe and Soderman's method (Rowe and Soderman 1985)

Variable	Test embankment	
	TE1	TE2
$(\gamma H_c)/S_u$ at failure – ninth layer	61.9/10	60.9/10
D/B	8.2/21	5.6/21
S_u/E_u	1/300	1/300
$\Omega = ((\gamma H_c)/S_u).(D/B).(S_u/E_u)$	0.0031	0.0013
ε_a % (Rowe and Soderman chart)	3.5	1.6
T (kN/m) using $J = 1700$ kN/m	59.5	27.2
Measured T (kN/m) at failure – ninth layer	40	50

γ_b = embankment bulk unit weight; H_c = critical embankment height (at failure); $S_u = 10$ kPa; D = depth of failure; B = width of the failure region.

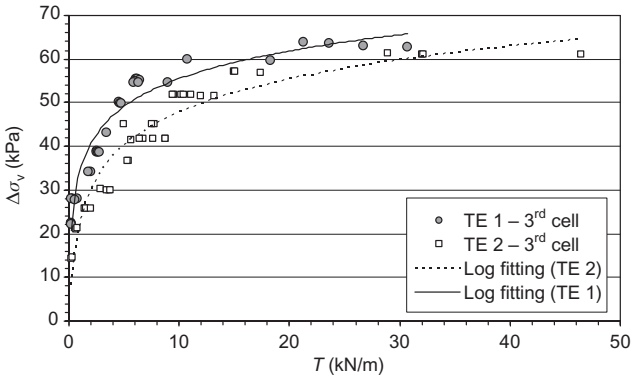

Figure 13. Embankment loading plotted against reinforcement forces measured at the third load cell

tions were 2.5 and 1.5% for embankments TE1 and TE2, respectively, and thus the horizontal direction hypothesis was well justified. The estimations of the gain in strength mentioned above were not considered, as the usual procedure for stability analyses of one-step constructed embankments is not to consider the gain in strength (Bjerrum 1972), and the same procedure was adopted herein.

4.2. Computed factors of safety

Stability analyses were carried out using the modified Bishop method, as the monitoring data and field evidence indicated circular failure surfaces. The field evidence indicated that the embankment failures were three-dimensional (3D), and thus the correction proposed by Azzouz *et al*. (1983) was implemented. Therefore, factors of safety FS_{3D} for the 3D condition were computed using the equation

$$\frac{FS_{3D}}{FS_{2D}} = \left(1 + 0.7\frac{DR}{2L}\right) \tag{2}$$

where FS_{2D} is the two-dimensional standard factor of safety, DR is the thickness of the failed region, and $2L$ is the width of the failed region. Values of DR and $2L$ obtained from the field observations and geometric data are shown in Table 6, together with the 3D correction factors obtained using equation 2.

The Bjerrum correction factor μ (Bjerrum 1972) was computed by trial and error until a factor of safety close to unity (assuming the 3D condition) was obtained for the failure condition (the ninth layer of the two embankments). Thus, different values of μ were multiplied by the S_u values shown in Figure 1. These computations resulted in a value for μ close to 0.60, and the critical failure surfaces obtained for embankments TE1 and TE2 are shown in Figure 14 together with the vertical deviation curves of the three inclinometers. Overall consistency between the critical surfaces and maximum vertical deviation values was observed.

Table 6. Correction due to three-dimensional effects (Azzouz *et al.* 1983)

Test embankment	DR (m)	$2L$ (m)	FS_{3D}/FS_{2D}
TE1	8.7	50	1.12
TE2	7.4	50	1.10

The variation in the factor of safety (using $\mu = 0.60$) with the embankment loading $\Delta\sigma_v$ is shown in Figure 15 for the two embankments. It was observed that the factors of safety for the two embankments were quite close in all the loading steps, which suggests again that the two embankments had similar behaviour.

It can also be seen in Figure 15 that the factors of safety for which the failures occurred are not exactly equal to unity (assuming $\mu = 0.60$ and failure in the ninth layer). The range of values of μ which yielded values of $FS_{3D} = 1.0$ is shown in Figure 16 together with other Brazilian case histories (Sandroni 1993). The relevant plasticity index for the present case is $I_p = 80\%$. Values of μ were also computed for the tenth layer for the two embankments, bearing in mind that the failure was identified visually in the tenth layer, although measurements indicated the ninth layer as the failure condition. Figure 16 also presents the relationship proposed by Azzouz *et al*. (1983), which is valid for 3D failures, and it can be seen that the values obtained in the present study (for the ninth and tenth layers) are consistent with the authors' curve.

5. REINFORCEMENT FORCES, FACTOR OF SAFETY, AND SHEARING BEHAVIOUR

Figure 17 shows the relationship between the factor of safety and the reinforcement force T. The values of T correspond to the measured values at the load cell located close to the failure surface (third load cell) after the fourth layer of embankment construction, as measurements for the first three layers resulted in quite small values of T. Note that the values of T increase with the decrease in the factor of safety and only values of F_s lower than 1.2 have mobilised significant values of T.

Figure 18 shows the relationship between the inverse

Table 5. Parameters adopted in stability analyses

	Embankment and sand layer working platform	Soft clay
Bulk unit weight (kN/m^3)	17.5	14.0–15.0
Strength parameters	$c = 0$; $\phi = 33.8^o$	see Figure 1
Reinforcement forces	Values measured in each load cell in each loading stage	

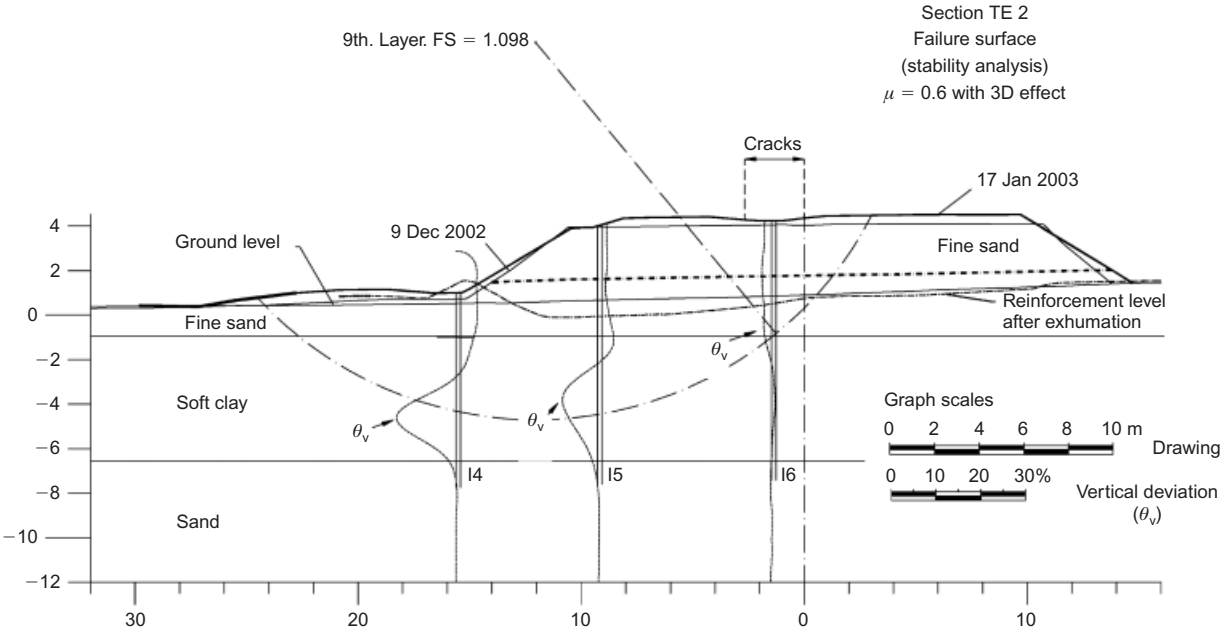

Figure 14. Failure surface obtained in stability analyses and measured vertical deviation (θ_v) measured in inclinometers

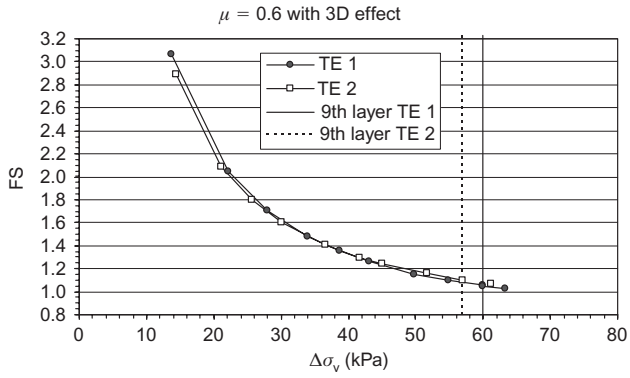

Figure 15. Factor of safety plotted against embankment loading for embankments TE1 and TE2

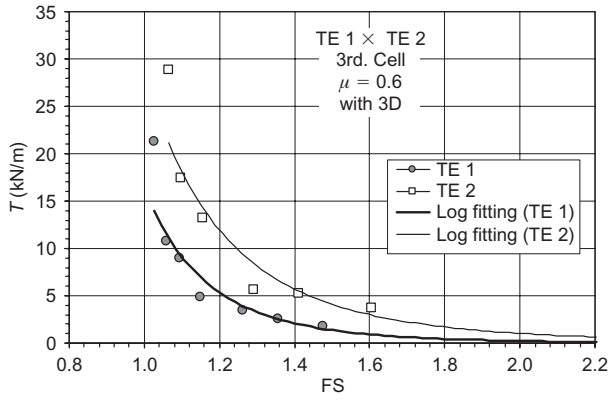

Figure 17. Measured reinforcement forces plotted against factor of safety for test embankments TE1 and TE2

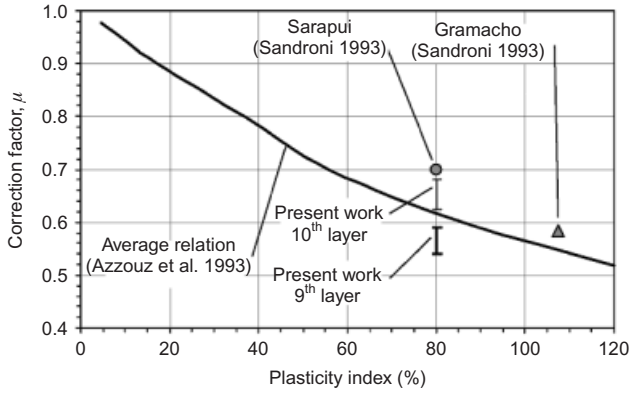

Figure 16. Correction factor plotted against plasticity index: case histories and Azzouz *et al*. (1983) relationship

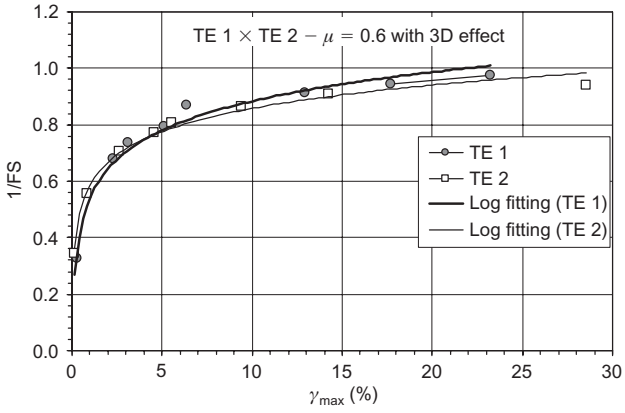

Figure 18. Inverse of the factor of safety plotted against maximum angular distortion for test embankments TE1 and TE2

of the factor of safety and the angular distortion γ mobilized in situ (see Figure 9). Fitting curves are also included in Figure 17 for the data of the two embankments and, as for Figure 6, the shapes of these curves are similar to the shape of stress–strain curves measured in undrained triaxial tests in normally consolidated clays. These data suggest that the shearing behaviours of the two embankments were quite similar. Therefore, the small gain in undrained strength of the clay under embankment TE1 with drains might not be significant enough to markedly differentiate the behaviours of the two embankments. Although the factors of safety and shearing behaviours of the two embankments were similar, higher values of reinforcement forces T were measured in embankment TE2, which appear to be related to the clay layer being thinner than that of embankment TE1.

6. CONCLUSIONS

Two reinforced test embankments, TE1 and TE2, were built on soft normally consolidated clay layers. Embankment TE1 was provided with vertical drains to simulate the conditions of a real engineering construction.

The mobilised tension forces (T) in reinforcements were shown to increase with the embankment height. Larger values of T were measured in embankment TE2, built on a shallower clay layer, which also presented larger values of vertical deviation measured by the inclinometers. The relationship between the maximum reinforcement forces T_{max} and maximum vertical deviation θ_{max} measured by the inclinometers located at the embankment toe was found to be linear for the two embankments. This linear relationship appears to be valid for service to failure conditions and also for the embankment provided with vertical drains.

The curves of vertical deviation plotted against time showed changes in the curvature that coincided with the instant in which cracks appeared in both embankments. A change of curvature, although with a smaller gradient, was also noticed in the curves of maximum reinforcement forces plotted against time.

The curves of embankment loading versus maximum vertical deviation were quite similar for the two embankments, and were also similar in shape to the stress–strain curves of undrained triaxial tests performed in normally consolidated clays.

Critical failure surfaces obtained in corrected limit equilibrium stability analyses were close to the observed field failure surfaces for 3D effects. These analyses used measured reinforcement forces resulting in Bjerrum correction factors around $\mu = 0.60$, which were similar to the relationship for 3D failures proposed in the literature by Azzouz *et al*. (1983). The two reinforced embankments presented similar factors of safety in all the loading stages, although one of them was built over a thicker layer of clay and was provided with vertical drains. The reinforcement loads increased with the decrease in the factor of safety.

ACKNOWLEDGEMENTS

The authors are indebted to all the individuals and institutions that have made the construction of the two test embankments possible, in particular the technical staff of COPPE-UFRJ Geotechnical Laboratory for the installation of the instruments. E. Marques made important comments on the final version. B. Lima helped in the editing of the paper and preparation of the figures.

NOTATIONS

Basic SI units are given in parentheses.

c	cohesion (Pa)
c_v	coefficient of vertical consolidation (m/s^2)
DR	thickness of the failed region (m)
e	void ratio (dimensionless)
FS	factors of safety (dimensionless)
h	embankment height (m)
I_P	plasticity index (dimensionless)
J	reinforcement modulus $= T/\varepsilon_a$ (N/m)
L	mid width of the failed region (m)
N_{kt}	empirical cone factor (dimensionless)
q_T	corrected point resistance (Pa)
S_u	undrained clay strength (Pa)
T	tension force at the reinforcement (N/m)
T_{max}	maximum tension force at the reinforcement (N/m)
Z	depth (m)
W	water content (dimensionless)
w_P	liquidity index (dimensionless)
δ_h	horizontal displacements (m)
ε_a	reinforcement strains (dimensionless)
ϕ	friction angle (degrees)
γ	distortion (dimensionless)
γ_b	bulk unit weight (N/m^3)
μ	Bjerrum correction factor (dimensionless)
θ_h	horizontal deviation (dimensionless)
θ_v	vertical deviation (dimensionless)
θ_{max}	maximum vertical deviation (dimensionless)
σ_v	total vertical stress (Pa)

REFERENCES

Azzouz, A. S., Baligh, M. M. & Ladd, C. C. (1983). Corrected field vane strength for embankment design. *Journal of Geotechnical Engineering ASCE*, **109**, No. 5, 730.

Bergado, D. T., Lorenzo, G. A. & Long, P. V. (2002). Limit equilibrium method back analyses of geotextile-reinforced embankments on soft Bangkok clay – a case study. *Geosynthetics International*, **9**, No. 3, 217–245.

Bjerrum, L. (1972). Embankments on soft ground. *Proceedings of the Special Conference on Performance of Earth and Earth-Supported Structures*, Purdue University, West Lafayette, IN, USA, ASCE, Reston, VA, USA, vol. 2, pp. 1–54.

Bonaparte, R. & Christopher, B. R. (1987). Design and construction of reinforced embankments over weak foundations. *Symposium on Reinforced Layered Systems*. Transportation Research Record 1153, pp. 26–39, TRB, Washington, DC, USA.

Davis, E. H. & Booker, J. R. (1973). The effect of increasing strength

with depth on the bearing capacity of clays. *Geotechnique*, **23**, No. 4, 551–563.

Houlsby, G. T. & Jewell, R. A. (1988). Analysis of reinforced and unreinforced embankments on soft clays by plasticity theory. *Proceedings of International Conference on Numerical Methods in Geomechanics*, Innsbruck, Austria, Balkema, Rotterdam, The Netherlands, vol. 2, pp. 1443–1448.

Jewell, R. A. (1992). A limit equilibrium design method for reinforced embankments on soft soils. *Proceedings of 2nd International Conference on Geotextiles*, Las Vegas, NV, USA, Industrial Fabrics Association International, Roseville, MN, USA, vol. 2 pp. 671–676.

Jewell, R. A. (1996). *Soil Reinforcements with Geotextiles*. Thomas Telford, London, UK. Construction Industry Research and Information Association, CIRIA Special publication 123.

John, N. W. M. (1987). *Geotextiles*. Blackie and Son, London, UK.

Kaniraj, S. R. (1994). Rotational stability of unreinforced and reinforced embankments on soft soils. *Journal of Geotextiles and Geomembranes*, **13**, No. 11, 707–726.

Leshchinsky, D. (1987). Short-term stability of reinforced embankment over clayey foundation. *Soils and Foundations*, **27**, No. 3, 43–57.

Li, A. L. & Rowe, R. K. (2001). Influence of creep and stress-relaxation of geosynthetic reinforcement on embankment behaviour. *Geosynthetics International,* **8**, No. 3, 233–270.

Long, P. V., Bergado, D. T. & Balasubramaniam, A. S. (1996). Stability analysis of reinforced and unreinforced embankments on soft ground. *Geosynthetics International,* **3**, No. 5, 583–604.

Low, B. K., Wong, K. S. & Lim, C. (1990). Slip circle analysis of reinforced embankment on soft ground. *Journal of Geotextiles and Geomembranes*, **9**, No. 2, 165–181.

Lunne, T., Robertson, P. K. & Powell, J. J. M. (1997). *Cone Penetration Testing in Engineering Practice*. Blackie Academic & Professional, London.

Magnani, H. (2006). *Behaviour of Reinforced Embankments on Soft Clays taken to Failure* (in Portuguese), DSc thesis. COPPE/UFRJ, Rio de Janeiro, RJ, Brazil.

Milligan, V. & Busbridge, J. R. (1983). Guidelines for the use of Tensar in reinforcement of fills over weak foundations. In: *Golder Associates Report to the Tensar Corp.*, Mississauga, Ontario, Canada.

Rowe, R. K. & Li, A. L. (2005). Geosynthetic-reinforced embankments over soft foundations. *Geosynthetics International*, **12**, No. 1, 50–85.

Rowe, R. K. & Soderman, K. L. (1985). An approximate method for estimating the stability of geotextile embankments. *Canadian Geotechnical Journal*, **22**, No. 3, 392–398.

Sandroni, S. S. (1993). On the use of vane tests in the design of embankments on soft clays. (in Portuguese), *Solos e Rochas*, **16**, No. 3, 207–213.

Saramago, R. P. (2002). *The Influence of the Soil Compaction in Reinforced Walls* (in Portuguese), DSc thesis. Graduate School of Engineering, Federal University of Rio de Janeiro, Brazil.

Saramago, R. P. & Ehrlich, M. (2005). Physical 1 : 1 scale model studies on geogrid reinforced soil walls. *Proceedings of the Sixteenth International Conference on Soil Mechanics and Geotechnical Engineering*, Osaka, Japan, Millpress, Rotterdam, The Netherlands, vol. 2, pp. 1405–1408.

Tavenas, F., Mieussens, C. & Bourges, F. (1979). Lateral displacements in clay foundation under embankments. *Canadian Geotechnical Journal*, **16**, No. 3, 532–550.

Shukla, S. K. & Kumar, R. (2008). Overall slope stability of prestressed geosynthetic-reinforced embankments on soft ground. *Geosynthetics International*, **15**, No. 2, 165–171.

Tanchaisawat, T., Bergado, D. T. & Voottipruex, P. (2008). Numerical simulation and sensitivity analyses of full-scale test embankment with reinforced lightweight geomaterials on soft Bangkok clay. *Geotextiles and Geomembranes*, **26**, No. 6, 498–511.

The Editor welcomes discussion on all papers published in Geosynthetics International. Please email your contribution to discussion@geosynthetics-international.com by 15 December 2009.